Influence of 3D Earth structure on Glacial Isostatic Adjustment in the Russian Arctic

Tanghua Li[1], Nicole S. Khan[2], Alisa V. Baranskaya[3], Timothy A. Shaw[1,4], W. Richard Peltier[5], Gordan R. Stuhne[5], Patrick Wu[6], and Benjamin P. Horton[1,4]

[1]Earth Observatory of Singapore, Nanyang Technological University, Singapore 639798, Singapore

[2]Department of Earth Sciences and the Swire Institute of Marine Science, University of Hong Kong, Hong Kong

[3]Lomonosov Moscow State University, Laboratory of Geoecology of the North, Moscow, Russia

[4]Asian School of the Environment, Nanyang Technological University, Singapore 639798, Singapore

[5]Department of Physics, University of Toronto, Toronto, Canada

[6]Department of Geoscience, University of Calgary, Alberta T2N 1N4, Canada

Corresponding author: Tanghua Li (li.tanghua@ntu.edu.sg/li.tanghua@connect.hku.hk)

Key Points:

- 1D GIA models ICE-6G_C (VM5a) and ICE-7G_NA (VM7) and 3D GIA models are validated with a quality-controlled deglacial Russian Arctic RSL database.
- 3D GIA model retains the good fits achieved by 1D models and improves the fits significantly in regions where 1D models show notable misfits.
- There is a compromise in the upper mantle between the background viscosity and scaling factor to best fit the deglacial RSL data.

Abstract

Analyses of glacial isostatic adjustment (GIA) and deglacial relative sea-level (RSL) change in the Russian Arctic deliver important insights into the Earth's viscosity structure and the deglaciation history of the Eurasian ice sheet complex. Here, we validate the latest iterations of 1D GIA models ICE-6G_C (VM5a) and ICE-7G_NA (VM7), and new 3D GIA models in the Russian Arctic against a quality-controlled deglacial RSL database of >500 sea-level data points from 24 regions. The 1D models correspond to the RSL data along the southern coast

of the Barents Sea and Franz-Josef-Land from ~11 ka BP to present but show notable misfits (> 50 m at 10 ka BP) with the White Sea data. We find 3D model predictions of deglacial RSL values are closer to the observed data than 1D models for the White Sea data while retaining comparable fits in other regions of the Russian Arctic. Our results reveal: (1) RSL in the western Russian Arctic is sensitive to elastic lithosphere with lateral thickness variation and 3D viscosity structure in the upper mantle; and (2) RSL in the whole Russian Arctic is less sensitive to 3D viscosity structure in the lower mantle compared to the upper mantle. The 3D models reveal a compromise in the upper mantle between the background viscosity and scaling factor to best fit the RSL data, which needs to be considered in future 3D GIA studies.

1 Introduction

Glacial isostatic adjustment (GIA) describes the dynamic response of the Earth's lithosphere and mantle to surface ice-water loading and unloading events, which makes a considerable contribution to relative sea-level (RSL) evolution since the Last Glacial Maximum (LGM) (e.g., Peltier, 1998; Whitehouse, 2018). Models of the GIA process (e.g., Argus et al., 2014; Lambeck et al., 1998, 2017; Peltier et al., 2015) link the cryosphere, hydrosphere, geosphere and atmosphere (e.g., Whitehouse, 2018; Wu et al., 2010), improve understanding of climate and sea-level changes by enabling reconstruction of ice-sheet histories (e.g., Lambeck et al., 2014; Milne & Mitrovica, 2008; Peltier et al., 2015) and provide important constraints on mantle rheology for the study of geodynamics (e.g., Huang et al., 2019; Lambeck et al., 2017; Peltier, 1998).

The search for an accurate GIA model of the Eurasian ice sheet complex is important for determination of viscosity structure and deglaciation history (e.g., Auriac et al., 2016; Patton et al., 2015; Steffen & Wu, 2011). The Eurasian ice sheet complex had the third largest ice mass during the LGM with a sea-level equivalent of ~20 m (e.g., Patton et al., 2017). Despite a long history of geologic studies (e.g., Forman et al., 2004; Kolka et al., 2015, 2013; Polyakova et al., 2005), reviews of deglacial RSL data in the Russian Arctic have only recently been conducted (Baranskaya, 2015; Makarov, 2017). Indeed, a new quality-controlled deglacial RSL database (Baranskaya et al., 2018) now offers an independent constraint for global GIA models and the testbed for the influence of 3D (i.e., laterally heterogeneous) Earth structure. The Russian Arctic database includes RSL information since the LGM from 26 regions with differing near- and intermediate field GIA histories.

Here we apply two state-of-the-art 1D global GIA models, ICE-6G_C (VM5a) (Argus et al., 2014; W R Peltier et al., 2015) and ICE-7G_NA (VM7) (Roy & Peltier, 2017, 2018) to test their performance in the Russian Arctic with the new RSL database (Baranskaya et al., 2018). Fixed with the ICE-6G_C ice history, we also study the influence of the 3D Earth structure on RSL predictions and search for an optimal 3D GIA model. Paulson et al. (2005) and Wang & Wu (2006) suggest that the 3D viscosity structures have the potential to better fit the deglacial RSL records both regionally and globally (e.g., Clark et al., 2019; Kuchar et al., 2019; Li et al., 2018). Indeed, previous GIA sensitivity tests suggest that RSL in the Russian Arctic region is sensitive to lateral variations in lithospheric thickness (Li & Wu, 2018; Zhong et al., 2003) and mantle viscosities (Li et al., 2018). We compare the predictions of 1D and 3D GIA models with deglacial RSL data to steer optimal 3D GIA model search strategy, guide future RSL data collection efforts and identify the regions where the local ice loading history employed in the 1D model was inadequately constrained. The modification of ice loading history might eliminate misfits of a 1D model to the deglacial RSL data.

2 RSL Data

We compare GIA model predictions to the deglacial RSL database of Baranskaya et al. (2018) (B18) from the Russian Arctic (Figure 1). B18 is derived from a variety of sea-level indicators including isolation basins, raised beaches, and perennially frozen salt marshes (laidas). The database was compiled following standard protocol (Khan et al., 2019; Shennan et al., 2015), where each valid data point requires precise knowledge of 1) the geographic location of the sample (i.e., its latitude and longitude); 2) the *in situ* age of the sample; 3) the elevation of the sample; and 4) the relationship of the indicator to sea level at its time of formation (i.e., indicative meaning; van de Plassche, 1986). We excluded a small number of samples from the B18 database that upon further scrutiny were found to be reworked or could not be reliably related to any tidal level. In addition, we did not use data from Kolka et al. (2013) and Kolka et al. (2015) (regions 5 and 9 of B18) older than 11.4 ka BP because it reflects local-scale effects related to the complex history of the White Sea ice lake (Hughes et al., 2016; Patton et al., 2017) that would not be resolved by the GIA models. After the data exclusion, the 26 regions in B18 became 24 regions (Figure 1a, b); the division is based on the relative influence of GIA, tectonic setting, and local geomorphological conditions.

The Russian Arctic database covers the Russian coasts of the White, Barents, Kara and Laptev seas. It contains 353 sea-level index points (SLIPs), which define the discrete position

of RSL in time and space, and 92 terrestrial and 78 marine limiting points, which provide an upper or lower bound on RSL in time and space, respectively (Engelhart & Horton, 2012).

3 GIA Modelling

We compare the RSL database to 1D and 3D GIA models. The 1D GIA models, ICE-6G_C (VM5a) (Argus et al., 2014; W R Peltier et al., 2015) and ICE-7G (VM7) (Roy & Peltier, 2017, 2018) were computed using the Normal Mode Method (NMM) and truncated at degree and order 512, where the horizontal resolution is comparable to 0.5 × 0.5-degree on the surface. The 3D GIA models were computed using the Coupled Laplace-Finite Element (CLFE) method (Wu, 2004) with 0.5 × 0.5-degree horizontal resolution near the surface, decreasing with depth to 2.0 × 2.0-degree in the lower mantle to reduce computational resources. Both 1D and 3D models consider the effects of rotational feedback and time dependent coastlines in the computation of the solution to the sea-level equation (Peltier, 1994). Note that the RSL prediction computed with CLFE method has been benchmarked with NMM for ICE-6G_C (VM5a) model before (Text S2 in Li et al., 2020).

The methodology for the 1D models is described in Peltier et al. (2015). For the 3D model, the 3D viscosity structure $\eta(r,\theta,\phi)$ is assumed to be the superposition of radial (η_o) and lateral viscosity structures ($\Delta\eta(r,\theta,\phi)$) logarithmically (Wang et al., 2008) in the form:

$$\log_{10}[\eta(r,\theta,\phi)] = \log_{10}[\eta_o] + \log_{10}[\Delta\eta(r,\theta,\phi)] \quad (1)$$

The radial viscosity structures were given by the background viscosity models (η_o). Lateral viscosity variations ($\Delta\eta(r,\theta,\phi)$) in the mantle were derived from the lateral shear velocity anomalies ($\frac{\delta v_s}{v_s}$) in TX2011 seismic tomography model (Grand, 2002) by employing the scaling relationship (Karato, 2008; Wu et al., 2013):

$$\log_{10}[\Delta\eta(r,\theta,\phi)] = \frac{-0.4343}{[\partial \ln v_s/\partial T]_{ah+an}} \frac{(E^*+pV^*)}{RT_0^2} \frac{\delta v_s}{v_s} \beta \quad (2)$$

where E^*, V^*, p, R and T_0 are the activation energy, activation volume, pressure, gas constant and background temperature profile, respectively. $[\partial \ln v_s/\partial T]_{ah+an}$ includes both the effects of anharmonicity (ah) and anelasticity (an). Here, we introduced parameter $\beta \in [0,1]$, which represents the fractional contribution of the thermal effect on seismic anomalies, and thus non-thermal effects such as chemical and non-isotropic pre-stress effects will consequently have the fractional contribution 1- β. We assumed that the β value in the two layers of the upper mantle (UM), UM1 and UM2, are the same (β_{UM}). Similar assumptions were made for the β value in lower mantle (LM), LM1 and LM2 (β_{LM}), accordingly. The elastic lithosphere

with lateral thickness variation were taken from Li & Wu (2018). It should be noted that TX2011 seismic tomography model (Grand, 2002) of the lateral heterogeneity of shear wave velocity has a lower resolution (2 × 2-degree) compared to the GIA model.

To guide 3D GIA model search strategy and future RSL data collection efforts, we defined locations that are optimally sensitive to 3D Earth structure (e.g., Steffen et al., 2014). The sensitivity of RSL to a specific parameter in a 3D model (i.e., an elastic lithosphere with lateral thickness variation, 3D viscosity structures in the upper mantle or lower mantle) was obtained from the difference between the RSL predictions of the 1D model (VM5a) and the 3D model, allowing only one parameter to vary at a time (Wu, 2006; Figure 2).

To define the optimal 3D model, we used the misfit χ-statistic (see details below describing how to calculate the misfit χ-statistic) to determine the parameters that achieved the best fit to the RSL data by first searching for the parameter space of the upper mantle, followed by the lower mantle. When searching for the optimal 3D upper mantle parameters, we set the lower mantle background viscosity to VM5a and the scaling factor (β_{LM}) to 0.6 (Li et al., 2018). We allowed the background viscosity in the upper mantle (η_{UM}) to vary between 0.01 $\times 10^{21}$ Pa s and 0.5 $\times 10^{21}$ Pa s (e.g., Auriac et al., 2016; Li et al., 2018) at 0.05 $\times 10^{21}$ Pa s interval (0.04 $\times 10^{21}$ Pa s interval from 0.01 to 0.05 $\times 10^{21}$ Pa s) and scaling factor in the upper mantle (β_{UM}) from 0 to 1 at a 0.1 interval (Figure 3a).

Next we searched for the optimal 3D structure in the lower mantle by allowing β_{LM} to vary from 0 to 1 at a 0.1 interval while keeping the 3D upper mantle fixed with our optimal values of η_{UM} and β_{UM} (Figure 3b). For lower mantle, we did not search for the background viscosity, which was fixed to VM5a because the RSL is less sensitive to lower mantle viscosity compared with the upper mantle in this region (e.g., Auriac et al., 2016; Steffen & Wu, 2011; Figure 2) and the 3D GIA model is computationally expensive (Li & Wu, 2018).

To evaluate the performance of 1D and 3D models, we generated GIA predictions at the unique location of each data point in the modified deglacial RSL database from B18 (Text S1 and Figure S1) and compared the predictions to each SLIP to calculate the misfit χ-statistics:

$$\chi = \sqrt{\frac{1}{N}\sum_{i=1}^{N}\left[\left[\frac{o_i - p_i(m_j)}{\Delta o_i}\right](t)\right]^2} \quad (3)$$

where N represents the number of data, o_i indicates ith observation with uncertainty Δo_i, and $p_i(m_j)$ are the ith prediction for model m_j (Wu et al., 2013). Following Tushingham & Peltier (1991), we account for the uncertainty Δt in the observation age by considering GIA

predictions at three times t and $t \pm \Delta t$ and choosing the value minimizing $\left[\left[\frac{o_i - p_i(m_j)}{\Delta o_i}\right](t)\right]^2$. The smaller the χ-statistics, the better the RSL predictions fit the deglacial RSL data.

4 Results and Discussion

4.1 1D GIA Models

The misfit χ-statistics for ICE-6G_C (VM5a) and ICE-7G_NA (VM7) compared to the deglacial RSL data are 5.13 and 4.45, respectively (Figure 1c). We attribute the better fit of the ICE-7G_NA (VM7) model pairing to the Earth model change from VM5a to VM7 rather than the ice loading histories because ICE-6G_C and ICE-7G_NA only differ slightly in North America and are identical elsewhere, including the Russian Arctic (Roy & Peltier, 2017).

Spatially, both ICE-6G_C (VM5a) and ICE-7G_NA (VM7) fit the RSL data along the southern coast of Barents Sea (regions 1-3) and the Franz-Josef-Land (region 19) (Figure 1c). However, they show notable misfits of up to 53 m at 10 ka BP in the White Sea (e.g., region 5, Figure 1c). The RSL predictions in the White Sea region lie above both the SLIPs and terrestrial limiting data older than ~6 ka BP. Such misfits may be eliminated by the incorporation of 3D structure in the lithosphere and mantle, because it shows notable shear velocity anomalies around White Sea (Figure S2) which indicates the potential necessity for 3D structure. In the absence of 3D structure, such misfits could be reduced by a thinner ice sheet or its earlier removal than represented in the ICE-6G_C/ICE-7G_NA ice loading histories (Tushingham & Peltier, 1992).

4.2 RSL Sensitivity Results

The patterns of RSL sensitivities to elastic lithosphere with lateral thickness variation and 3D viscosity structures in the upper and lower mantle remain stable through time, although the magnitudes decrease (Figure 2, S3, S4 and S5). RSL in the western Russian Arctic (regions 1 to 15) is sensitive to elastic lithosphere with lateral thickness variation and 3D viscosity structure in the upper mantle, which may address the notable misfits with 1D GIA models (e.g., White Sea coasts). The regions most sensitive to elastic lithosphere with lateral thickness variation and 3D viscosity structure in the upper mantle are the Barents Sea (regions 1-3) and the southwestern Kara Sea. Insufficient RSL data availability from the Kara Sea coasts (Baranskaya et al., 2018) limits possible constraints. Intriguingly, the accessible

RSL data for the west of the Kara Sea suggest a continuous fall from ~45 m at 11 ka BP to ~0.5 m at 0.5 ka BP (e.g., region 19), whereas the east of the Kara Sea shows continuous RSL rise from around -48 m at 11 ka BP to ~2 m at 1 ka BP (e.g., region 22) (Baranskaya et al., 2018). The deglacial RSL data of the Kara Sea, therefore, imply the region is near the forebulge and more RSL data would provide evidence for the position of deglacial ice margins (e.g., Tushingham & Peltier, 1991), which are poorly constrained currently (Patton et al., 2015, 2017).

RSL in the Russian Arctic is relatively insensitive to the 3D viscosity structure in the lower mantle because the ice sheet was not large enough to clearly resolve the lower mantle viscosity structure (e.g., Steffen & Wu, 2011; Wu et al., 2013).

4.3 3D GIA Models

We determined the preferred/optimal η_{UM} and β_{UM} in the upper mantle in the Russian Arctic (Figure 3a). When the upper mantle is 1D (i.e., β_{UM}=0), the RSL misfit χ-statistics reduces dramatically from 5.10 to 1.82 when η_{UM} increases from 0.01 to 0.2 $\times 10^{21}$ Pa s and expands from 1.83 to 2.96 when η_{UM} increases from 0.3 to 0.5 $\times 10^{21}$ Pa s. The preferred 1D η_{UM} is ~0.2-0.3 $\times 10^{21}$ Pa s, which is consistent with previous 1D viscosity inversion results using deglacial RSL data in Northern Europe (e.g., Lambeck et al., 1998; Lau et al., 2016; Mitrovica & Peltier, 1993) and in the Barents Sea region (e.g., Auriac et al., 2016).

With an increase of the scaling factor β_{UM}, the χ-statistics reduces when the $\eta_{UM} < 0.1 \times 10^{21}$ Pa s. The addition of a positive viscosity variation to such a low η_{UM} further improves the fit with the deglacial RSL data because the positive lateral shear velocity anomaly in the upper mantle (Figure S2) makes the lateral viscosity variation in the upper mantle positive (Equation 1 and 2, Figure S6). The misfit χ-statistic expands with the increase of $\beta_{UM}$when $\eta_{UM} > 0.3 \times 10^{21}$ Pa s because η_{UM} is already so high, adding a positive viscosity variation to η_{UM} will naturally deteriorate the fit to the RSL data (Li et al., 2018).

We find a compromise in the upper mantle between η_{UM} and β_{UM} (Figure 3a), which validates the hypothesis of Li et al. (2018) that there may be a trade-off between these two parameters. This compromise should be considered in future 3D GIA studies because it indicates that presuming $\beta = 1$ (e.g., Kuchar et al., 2019; Wang & Wu, 2006a) maybe not realistic, although it may improve the fit with relatively lower η_{UM} values (e.g., when $\eta_{UM} < 0.1 \times 10^{21}$ Pa s in this study). Also incorporating 3D structure may considerably deteriorate the fit with RSL data when using inappropriate values of η_{UM} (e.g., Li et al., 2018; when η_{UM}

$> 0.3 \times 10^{21}$ Pa s in this study). The substantial changes in the χ-statistics both horizontally (with η_{UM} variation) and vertically (with β_{UM} variation) in Figure 3a confirm that RSL predictions are sensitive to choices of the background viscosity model (e.g., Li et al., 2018; Wang & Wu, 2006b) and scaling factor (e.g., Clark et al., 2019; Wu et al., 2013) in the 3D Earth structure determination. The optimal model (χ = 1.44; red star in Figure 3a) is found with $\eta_{UM} = 0.1 \times 10^{21}$ Pa s and β_{UM}= 0.8.

We subsequently fixed the 3D viscosity structure in the upper mantle to the optimal model (red star in Figure 3a) and searched for the optimal scaling factor in the lower mantle (β_{LM}). The χ-statistics reduces with the increase of the scaling factor in the lower mantle (β_{LM}) and reaches the minimum of 1.41 when β_{LM}= 0.8 (optimal 3D model, red star in Figure 3b), then slightly expands with β_{LM}> 0.8. With β_{LM}=0.8, the negative shear velocity anomaly in LM1 (Figure S2b) causes the shallow lower mantle viscosity to decrease (Figure S6b) and the positive shear velocity anomaly in LM2 (Figure S2d) generates an increase in the deep lower mantle viscosity (Figure S6d). This is consistent with changing from VM5a to VM7 and improves the fit with the deglacial RSL data (Figure 1c).

The optimal 3D model (red star in Figure 3b) has a notably high viscosity value of ~3.5 $\times 10^{21}$ Pa s in UM1 and ~0.2 $\times 10^{21}$ Pa s in UM2 beneath the White Sea region with a decreasing gradient northwards (Figure S7a, S7c). Despite regional peaks in viscosities of the sublayers, the mean viscosity in the whole upper mantle is ~0.6 $\times 10^{21}$ Pa s around the White Sea and ~0.3 $\times 10^{21}$ Pa s around Franz-Josef-Land (Figure S7e), which is within reasonable range of the suggested upper mantle viscosity that did not differentiate distinct layers in the upper mantle (e.g., Auriac et al., 2016; Steffen & Wu, 2011).

We compare the RSL predictions of the 1D model ICE-6G_C (VM5a) and the optimal 3D model with the RSL data at 9 regions, where RSL histories are well-constrained (Figure 4). The 3D model significantly improves the fit with the RSL data around the White Sea, where 1D models show notable misfits (Figure 1c). For example, the misfit at region 5 at ~10 ka BP reduces from over 50 m using ICE-6G_C (VM5a) to less than 5 m using the optimal 3D model (region 5 in Figure 4). The RSL predictions from the 3D model at all regions around the White Sea are all below the predictions of ICE-6G_C (VM5a) because of the incorporation of elastic lithosphere with lateral thickness variation and 3D viscosity structure both in the upper and lower mantle. Meanwhile, the optimal 3D model can retain the good fits that 1D models achieved along the southern coast of Barents Sea (regions 1-3) and the

Franz-Josef-Land (region 19). The remaining misfits in White Sea (e.g., region 10, 11) imply that the ice history of ICE-6G_C around the White Sea region may need to be refined. Indeed, Auriac et al. (2016) concluded that the ice thickness around Barents Sea of ICE-6G_C might be overestimated.

5 Conclusions

We validate the 1D GIA models ICE-6G_C (VM5a) (Argus et al., 2014; W R Peltier et al., 2015) and ICE-7G_NA (VM7) (Roy & Peltier, 2017, 2018) and 3D GIA models in the Russian Arctic with the further refined quality-controlled deglacial RSL database from Baranskaya et al. (2018). We have revealed RSL sensitivities to elastic lithosphere with lateral thickness variations and 3D Earth structures in the upper and lower mantle and have investigated the influence of 3D Earth structure on RSL predictions in the Russian Arctic. Comparison of RSL predictions with deglacial RSL data shows:

1. Both ICE-6G_C (VM5a) and ICE-7G_NA (VM7) fit the deglacial RSL data along the southern coast of the Barents Sea (regions 1-3) and around Franz-Josef-Land (region 19), while they show notable misfits around the White Sea (e.g., region 7, 9-11). ICE-7G_NA (VM7) has also been demonstrated to out-perform ICE-6G_C (VM5a).
2. The optimal 3D GIA model has β_{UM}= 0.8, $\eta_{UM} = 0.1 \times 10^{21}$ Pa s, β_{LM}= 0.8, η_{LM}, which is the same as that in VM5a and elastic lithosphere with lateral thickness variation from Li & Wu (2018). This model notably improves the fit to the deglacial RSL data around White Sea and retains the good fits that 1D models achieved along the southern coast of the Barents Sea and around Franz-Josef-Land.
3. There is a compromise in the upper mantle between the background viscosity and scaling factor to fit the deglacial RSL data, which needs to be considered in future 3D GIA studies.
4. RSL in the western Russian Arctic is sensitive to elastic lithospheric thickness and to the 3D viscosity structure in the upper mantle. The RSL in the Russian Arctic is relatively insensitive to 3D viscosity structure in the lower mantle.

In this study the uncertainties in ice model and correlation between the ice model and mantle viscosity are not considered. In the absence of this analysis, it remains undetermined whether the 3D structure achieved in this study to provide a better fit with the deglacial RSL data is related to the real 3D structure of the mantle and lithosphere or results from uncertainties of the ice model. The introduction of lateral viscosity heterogeneity adds additional degrees (e.g.,

β_{UM} and β_{LM}) of freedom to the GIA model. All these caveats suggest the necessity of continuing to update the GIA study in the Russian Arctic.

Acknowledgments

Tanghua Li, Timothy A. Shaw and Benjamin P. Horton are supported by the Singapore Ministry of Education Academic Research Fund MOE2019-T3-1-004 and MOE2018-T2-1-030, the National Research Foundation Singapore, and the Singapore Ministry of Education, under the Research Centers of Excellence initiative. The research of W. Richard Peltier at Toronto is supported by NSERC discovery Grant A9627. The work of Alisa Baranskaya was supported by the Russian Foundation for Basic Research grant 20-35-70002; she used equipment and facilities obtained within the State Budget Theme AAAA-A16-116032810055-0. The FE calculation was performed with the ABAQUS package from Hibbitt, Karlsson and Sorensen Inc. This research is conducted in part using the research computing facilities and/or advisory services offered by Information Technology Services, the University of Hong Kong. The authors acknowledge HOLSEA and PALSEA, working groups of the International Union for Quaternary Sciences (INQUA) and Past Global Changes (PAGES), which in turn received support from the Swiss Academy of Sciences and the Chinese Academy of Sciences. This article is a contribution to International Geoscience Program (IGCP) Project 639, “Sea-Level Changes from Minutes to Millennia”. This work is Earth Observatory of Singapore contribution XXX. The deglacial RSL data used in this study is from the supplementary information of Baranskaya et al. (2018) (with link) that is listed in the References List.

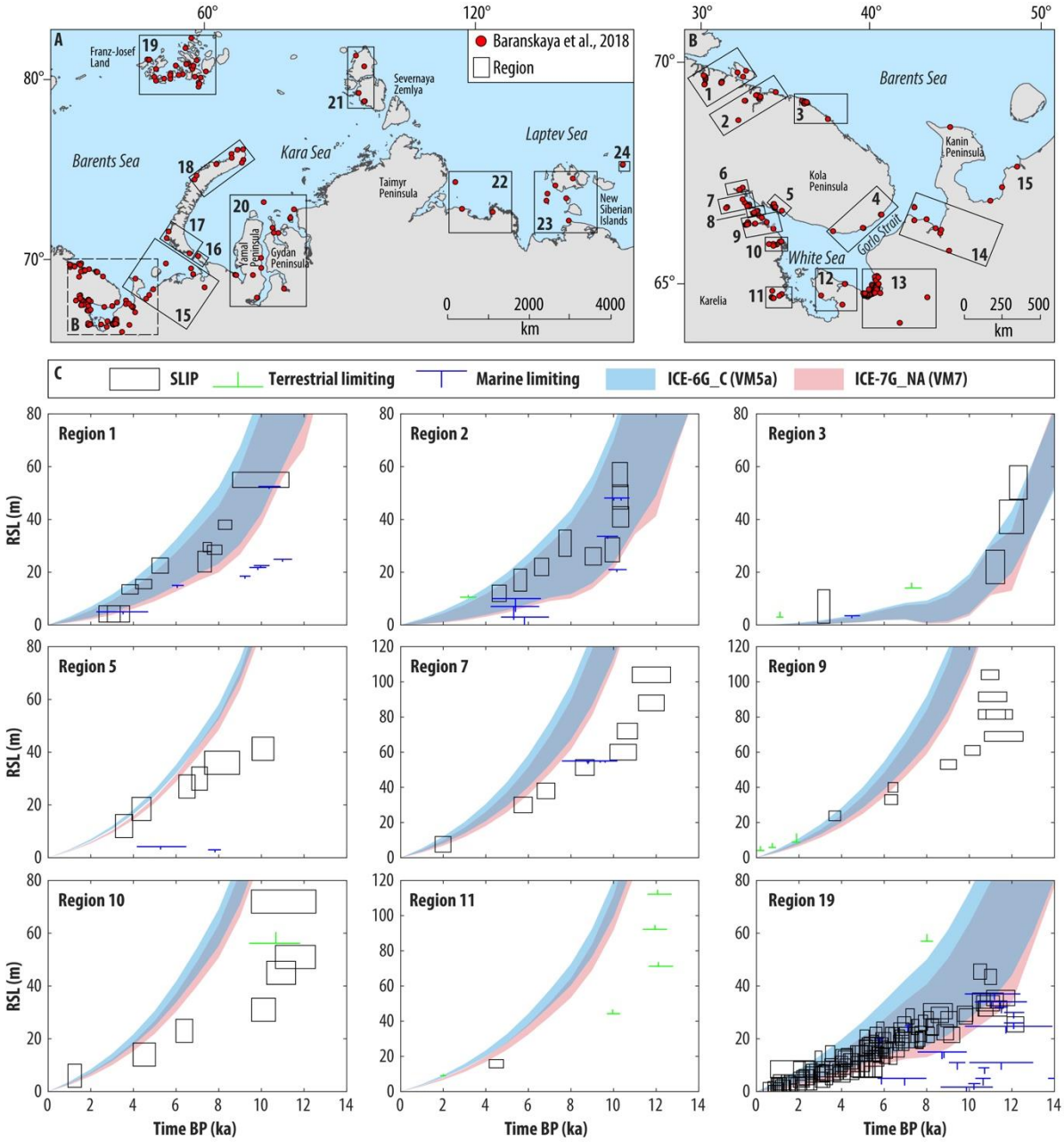

Figure 1. Russian Arctic study region and revised deglacial relative sea-level (RSL) database modified after Baranskaya et al. (2018) showing regions (a) 15-24 and (b) 1-14. (c) RSL predictions from 1D glacial isostatic adjustment models ICE-6G_C (VM5a) and ICE-7G_NA (VM7) at 9 selected regions compared with deglacial RSL data. Sea level index points are plotted as boxes with 2σ vertical and calibrated age errors. Terrestrial and marine limiting data provide upper and lower constraints on RSL, respectively.

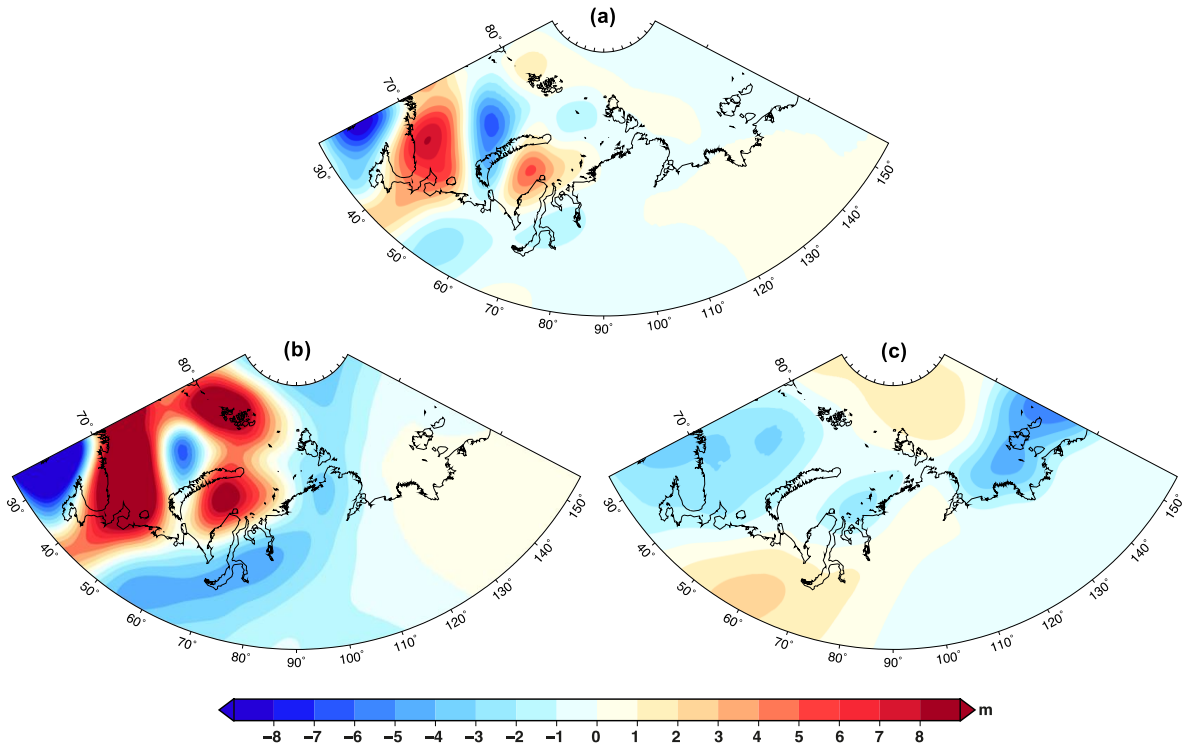

312

313 Figure 2. The relative sea-level (RSL) sensitivity to (a) elastic lithosphere with lateral
314 thickness variation and 3D viscosity structures in (b) the upper mantle and (c) the lower
315 mantle at 4 ka BP. The RSL sensitivity maps at 12, 8 and 1 ka BP are shown in Figures S3,
316 S4 and S5.

317

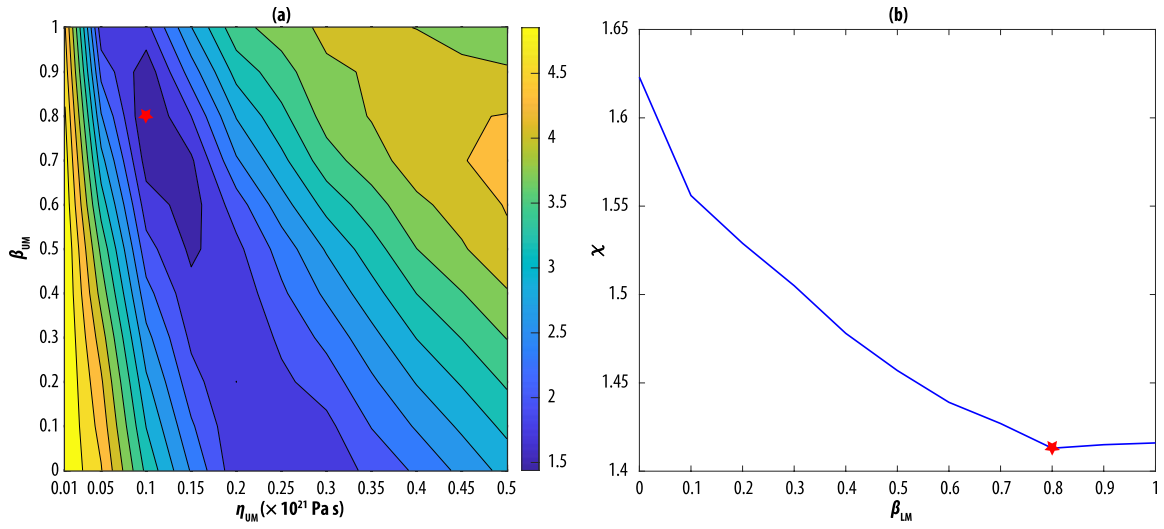

318

319 Figure 3. (a) The relative sea-level (RSL) misfit χ-statistics with varying upper mantle
320 background viscosity (η_{UM}) and scaling factor (β_{UM}). The red star in (a) represents the
321 smallest χ in a. (b) χ statistics with varying scaling factor in the lower mantle (β_{LM}) fixed

with the optimal parameters of the red start in (a) in the upper mantle. The red star in b represents the smallest χ (optimal 3D glacial isostatic adjustment model) in b. The background viscosity in the lower mantle (η_{LM}) is the same as that in VM5a.

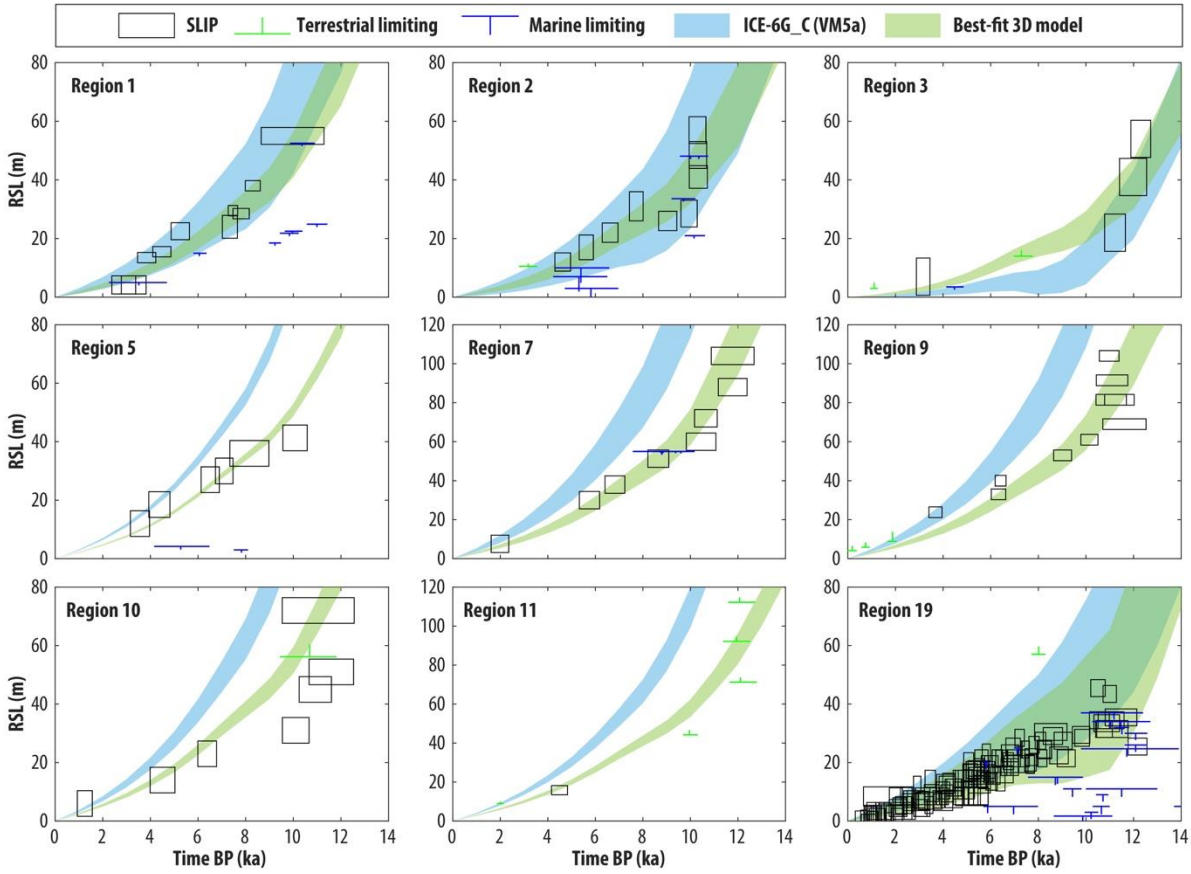

Figure 4. Relative sea-level (RSL) predictions from 1D glacial isostatic adjustment model ICE-6G_C (VM5a) and the optimal 3D model at 9 selected regions as per Figure 1 compared with deglacial RSL data.

References

Argus, D. F., Peltier, W. R., Drummond, R., & Moore, A. W. (2014). The Antarctica component of postglacial rebound model ICE-6G_C (VM5a) based on GPS positioning, exposure age dating of ice thicknesses, and relative sea level histories. *Geophysical Journal International*, *198*(1), 537–563.

Auriac, A., Whitehouse, P. L., Bentley, M. J., Patton, H., Lloyd, J. M., & Hubbard, A. (2016). Glacial isostatic adjustment associated with the Barents Sea ice sheet: a modelling inter-comparison. *Quaternary Science Reviews*, *147*, 122–135.

Baranskaya, A.V., 2015. The role of the latest tectonic movements in the formation of the relief of the coasts of the Russian Arctic. Summary of the thesis for a degree of Doctor of Philosophy (geographical science), speciality 25.00.25 - geomorphology and evolutional geography. PhD thesis, Saint Petersburg State University. Saint-Petersburg. pp. 26. (In Russian)

Baranskaya, A. V, Khan, N. S., Romanenko, F. A., Roy, K., Peltier, W. R., & Horton, B. P. (2018). A postglacial relative sea-level database for the Russian Arctic coast. *Quaternary Science Reviews*, *199*, 188–205. https://doi.org/10.1016/j.quascirev.2018.07.033 Accessed 2020-07-15

Clark, J., Mitrovica, J. X., & Latychev, K. (2019). Glacial isostatic adjustment in central Cascadia: Insights from three-dimensional Earth modeling. *Geology*, *47*(4), 295–298.

Engelhart, S. E., & Horton, B. P. (2012). Holocene sea level database for the Atlantic coast of the United States. *Quaternary Science Reviews*, *54*, 12–25.

Forman, S. L., Lubinski, D. J., Ingólfsson, Ó., Zeeberg, J. J., Snyder, J. A., Siegert, M. J., & Matishov, G. G. (2004). A review of postglacial emergence on Svalbard, Franz Josef Land and Novaya Zemlya, northern Eurasia. *Quaternary Science Reviews*, *23*(11–13), 1391–1434.

Grand, S. P. (2002). Mantle shear–wave tomography and the fate of subducted slabs. *Philosophical Transactions of the Royal Society of London. Series A: Mathematical, Physical and Engineering Sciences*, *360*(1800), 2475–2491.

Huang, P., Wu, P., & Steffen, H. (2019). In search of an ice history that is consistent with composite rheology in Glacial Isostatic Adjustment modelling. *Earth and Planetary Science Letters*, *517*, 26–37.

Hughes, A. L. C., Gyllencreutz, R., Lohne, Ø. S., Mangerud, J., & Svendsen, J. I. (2016). The last Eurasian ice sheets–a chronological database and time-slice reconstruction, DATED-1. *Boreas*, *45*(1), 1–45.

Karato, S. I. (2008). *Deformation of Earth materials. An introduction to the rheology of Earth materials*. Cambridge Univ. Press, ISBN.

Khan, N. S., Horton, B. P., Engelhart, S., Rovere, A., Vacchi, M., Ashe, E. L., Törnqvist, T. E., Dutton, A., Hijma, M. P., & Shennan, I. (2019). Inception of a global atlas of sea levels since the Last Glacial Maximum. *Quaternary Science Reviews*, *220*, 359–371.

Kolka, V. V, Korsakova, O. P., Shelekhova, T. S., Lavrova, N. B., & Arslanov, K. A. (2013). Reconstruction of the relative level of the White Sea during the Holocene on the Karelian coast near Engozero settlement, Northern Karelia. *Doklady Earth Sciences*, *449*(2), 434–438.

Kolka, V. V, Korsakova, O. P., Shelekhova, T. S., & Tolstobrova, A. N. (2015). Reconstruction of the relative level of the White Sea during the Late Glacial–Holocene according to lithological, diatom analyses and radiocarbon dating of small lakes bottom sediments in the area of the Chupa settlement (North Karelia, Russia). *Vestnik of MGTU*, *18*(2), 255–268.

Kuchar, J., Milne, G., & Latychev, K. (2019). The importance of lateral Earth structure for North American glacial isostatic adjustment. *Earth and Planetary Science Letters*, *512*, 236–245.

Lambeck, K., Purcell, A., & Zhao, S. (2017). The North American Late Wisconsin ice sheet and mantle viscosity from glacial rebound analyses. *Quaternary Science Reviews*, *158*, 172–210.

Lambeck, K., Rouby, H., Purcell, A., Sun, Y., & Sambridge, M. (2014). Sea level and global ice volumes from the Last Glacial Maximum to the Holocene. *Proceedings of the National Academy of Sciences*, *111*(43), 15296–15303.

Lambeck, K., Smither, C., & Johnston, P. (1998). Sea-level change, glacial rebound and mantle viscosity for northern Europe. *Geophysical Journal International*, *134*(1), 102–144.

Lau, H. C. P., Mitrovica, J. X., Austermann, J., Crawford, O., Al-Attar, D., & Latychev, K. (2016). Inferences of mantle viscosity based on ice age data sets: Radial structure. *Journal of Geophysical Research: Solid Earth*, *121*(10), 6991–7012.

Li, T., & Wu, P. (2018). Laterally heterogeneous lithosphere, asthenosphere and sub-lithospheric properties under Laurentia and Fennoscandia from Glacial Isostatic Adjustment. *Geophysical Journal International*, *216*(3), 1633–1647.

Li, T., Wu, P., Steffen, H., & Wang, H. (2018). In search of laterally heterogeneous viscosity models of glacial isostatic adjustment with the ICE-6G_C global ice history model. *Geophysical Journal International*, *214*(2), 1191–1205.

Li, T., Wu, P., Wang, H., Steffen, H., Khan, N. S., Engelhart, S. E., Vacchi, M., Shaw, T. A., Peltier, W. R., & Horton, B. P. (2020). Uncertainties of Glacial Isostatic Adjustment model predictions in North America associated with 3D structure. *Geophysical Research Letters*, e2020GL087944.

Makarov, A.S. 2017. Changes in the level of Arctic seas in the Holocene. Summary of a Dr. Hab. thesis in Geographical Science Summary of the thesis for a degree of Doctor of Philosophy (geographical science), speciality 25.00.25 - geomorphology and evolutional geography. PhD thesis, Saint Petersburg State University. Saint-Petersburg. 45 pp. (In Russian)

Milne, G. A., & Mitrovica, J. X. (2008). Searching for eustasy in deglacial sea-level histories. *Quaternary Science Reviews*, *27*(25–26), 2292–2302.

Mitrovica, J. X., & Peltier, W. R. (1993). The inference of mantle viscosity from an inversion of the Fennoscandian relaxation spectrum. *Geophysical Journal International*, *114*(1), 45–62.

Patton, H., Andreassen, K., Bjarnadóttir, L. R., Dowdeswell, J. A., Winsborrow, M. C. M., Noormets, R., Polyak, L., Auriac, A., & Hubbard, A. (2015). Geophysical constraints on the dynamics and retreat of the Barents Sea ice sheet as a paleobenchmark for models of marine ice sheet deglaciation. *Reviews of Geophysics*, *53*(4), 1051–1098.

Patton, H., Hubbard, A., Andreassen, K., Auriac, A., Whitehouse, P. L., Stroeven, A. P., Shackleton, C., Winsborrow, M., Heyman, J., & Hall, A. M. (2017). Deglaciation of the Eurasian ice sheet complex. *Quaternary Science Reviews*, *169*, 148–172.

Peltier, W R. (1998). Postglacial variations in the level of the sea: Implications for climate dynamics and solid-earth geophysics. *Reviews of Geophysics*, *36*(4), 603–689.

Peltier, W R, Argus, D. F., & Drummond, R. (2015). Space geodesy constrains ice age terminal deglaciation: The global ICE-6G_C (VM5a) model. *Journal of Geophysical Research: Solid Earth*, *120*(1), 450–487.

Peltier, W Richard. (1994). Ice age paleotopography. *Science*, *265*(5169), 195–201.

Polyakova, Y. I., Bauch, H. A., & Klyuvitkina, T. S. (2005). Early to middle Holocene changes in Laptev Sea water masses deduced from diatom and aquatic palynomorph assemblages. *Global and Planetary Change*, *48*(1–3), 208–222.

Roy, K., & Peltier, W. R. (2017). Space-geodetic and water level gauge constraints on continental uplift and tilting over North America: Regional convergence of the ICE-6G_C (VM5a/VM6) models. *Geophysical Journal International*, *210*(2), 1115–1142.

Roy, K., & Peltier, W. R. (2018). Relative sea level in the Western Mediterranean basin: a regional test of the ICE-7G_NA (VM7) model and a constraint on late Holocene Antarctic deglaciation. *Quaternary Science Reviews*, *183*, 76–87.

Shennan, I., Long, A. J., & Horton, B. P. (2015). *Handbook of sea-level research*. John Wiley & Sons.

Steffen, H, Wu, P., & Wang, H. (2014). Optimal locations of sea-level indicators in glacial isostatic adjustment investigations. *Solid Earth*, *5*(1), 511.

Steffen, Holger, & Wu, P. (2011). Glacial isostatic adjustment in Fennoscandia---a review of data and modeling. *Journal of Geodynamics*, *52*(3), 169–204.

Tushingham, A. M., & Peltier, W. R. (1992). Validation of the ICE-3G Model of Würm-Wisconsin Deglaciation using a global data base of relative sea level histories. *Journal of Geophysical Research: Solid Earth*, *97*(B3), 3285–3304.

Tushingham, A., & Peltier, W. R. (1991). Ice-3G: A new global model of late Pleistocene deglaciation based upon geophysical predictions of post-glacial relative sea level change. *Journal of Geophysical Research: Solid Earth*, *96*(B3), 4497–4523.

Van de Plassche, O. (1986). Sea-level research: A manual for the collection and evaluation of data: Norwich. *UK*, *Geobooks*.

Wang, H., & Wu, P. (2006a). Effects of lateral variations in lithospheric thickness and mantle viscosity on glacially induced relative sea levels and long wavelength gravity field in a spherical, self-gravitating Maxwell Earth. *Earth and Planetary Science Letters*, *249*(3), 368–383.

Wang, H., & Wu, P. (2006b). Role of background viscosity in the investigation of postglacial rebound induced crustal motion in a laterally heterogeneous mantle. *Journal of Geodynamics*, *42*(1), 85–94.

Wang, H., Wu, P., & van der Wal, W. (2008). Using postglacial sea level, crustal velocities and gravity-rate-of-change to constrain the influence of thermal effects on mantle lateral heterogeneities. *Journal of Geodynamics*, *46*(3–5), 104–117.

Whitehouse, P. L. (2018). Glacial isostatic adjustment modelling: historical perspectives, recent advances, and future directions. *Earth Surface Dynamics.*, *6*(2), 401–429.

Wu, P. (2004). Using commercial finite element packages for the study of earth deformations, sea levels and the state of stress. *Geophysical Journal International*, *158*(2), 401–408.

Wu, P. (2006). Sensitivity of relative sea levels and crustal velocities in Laurentide to radial and lateral viscosity variations in the mantle. *Geophysical Journal International*, *165*(2), 401–413.

Wu, P., Steffen, H., & Wang, H. (2010). Optimal locations for GPS measurements in North America and northern Europe for constraining Glacial Isostatic Adjustment. *Geophysical Journal International*, *181*(2), 653–664.

Wu, P., Wang, H., & Steffen, H. (2013). The role of thermal effect on mantle seismic anomalies under Laurentia and Fennoscandia from observations of Glacial Isostatic Adjustment. *Geophysical Journal International*, *192*(1), 7–17.

Zhong, S., Paulson, A., & Wahr, J. (2003). Three-dimensional finite-element modelling of Earth's viscoelastic deformation: effects of lateral variations in lithospheric thickness. *Geophysical Journal International*, *155*(2), 679–695.